An Autoinhibitory Mechanism for Nonsyntaxin SNARE Proteins Revealed by the Structure of Ykt6p

Hidehito Tochio, *et al.*

Science **293**, 698 (2001);
DOI: 10.1126/science.1062950

Vector Control, C. F. Curtis, Ed. (CRC Press, Boca Raton, FL, 1990), p. 187.
29. U. Kitron, A. Spielman, *Rev. Infect. Dis.* **11**, 391 (1989).
30. S. K. Ault, *Am. J. Trop. Med. Hyg. Suppl.* **50**, 35 (1994).
31. Special Programme for Research and Training in Tropical Diseases, *Work plan of the task force on applied research on Chagas disease* (World Health Organization, Geneva, 1999). Available at: www.who.int/tdr/grants/workplans/chagas4.htm.
32. We thank A. E. Cohen, C. Dye, J. E. Rabinovich, C. J. Schofield, and B. H. Singer for helpful comments on a previous draft. We also thank the Rockefeller Foundation for grant RF 91080, Allocation 133. J.E.C. thanks the NSF for grants BSR 9207293 and DEB 9981552, and Mr. and Mrs. W. T. Golden for hospitality during this work. R.E.G. thanks the University of Buenos Aires, the Fulbright and Thalmann programs, and CONICET of Argentina for grants. The authors thank D. M. Canale, M. B. Castañera, I. Castro, M. C. Cecere, R. Chuit, A. Hurvitz, M. A. Lauricella, E. L. Segura, and D. P. Vázquez for sustained long-term commitment which made possible the empirical studies underlying the model.

12 March 2001; accepted 5 June 2001

An Autoinhibitory Mechanism for Nonsyntaxin SNARE Proteins Revealed by the Structure of Ykt6p

Hidehito Tochio,[1]* Marco M. K. Tsui,[2]* David K. Banfield,[2]† Mingjie Zhang[1]†

Ykt6p is a nonsyntaxin SNARE implicated in multiple intracellular membrane trafficking steps. Here we present the structure of the NH_2-terminal domain of Ykt6p (Ykt6pN, residues 1 to 140). The structure of Ykt6pN differed entirely from that of syntaxin and resembled the overall fold of the actin regulatory protein, profilin. Like some syntaxins, Ykt6p adopted a folded back conformation in which Ykt6pN bound to its COOH-terminal core domain. The NH_2-terminal domain plays an important biological role in the function of Ykt6p, which in vitro studies revealed to include influencing the kinetics and proper assembly of SNARE complexes.

The secretory pathway of eukaryotic cells is comprised of a number of distinct membrane-bound compartments between which proteins and lipids are transported in vesicles that pinch off from one membrane and fuse with another. Targeting and fusion of vesicles is mediated in part by specific interactions between integral membrane proteins on the vesicles and target organelles; these are soluble *N*-ethylmaleimide-sensitive factor attachment receptor proteins, termed v-SNAREs and t-SNAREs, respectively (*1*, *2*). However, a single SNARE can operate in more than one transport step as well as interact with several different SNARE binding partners (*3*). Previous structural studies have been restricted to the syntaxin SNARE family members (*4*–*11*). Here, we determined the atomic structure of Ykt6p, a nonsyntaxin SNARE in solution, by nuclear magnetic resonance (NMR) spectroscopy. We chose Ykt6p because it is an evolutionarily conserved protein that is involved in multiple intracellular transport steps and thus is likely to be subject to regulatory control (*12*–*14*).

Extensive experimental trials showed that full-length Ykt6p is not amenable to structural determination by NMR. Marked improvements in the quality of the NMR spectra were obtained for Ykt6p lacking the COOH-terminal core (the SNARE-SNARE binding domain, residues 141 to 200). The structure of the NH_2-terminal domain of Ykt6p (Ykt6pN, residues 1 to 140) was determined from a total of 2515 NMR-derived restraints (*15*). The backbone of Ykt6pN was well-defined (Fig. 1A) and consisted of five β strands and four α helices (Fig. 1B). The five β strands were arranged in an βII-βI-βV-βIV-βIII antiparallel β sheet, sandwiched by the αA and αB/αD helices (Fig. 1B). A short α helix (αC) in the linker region connected αB and αD. The overall fold of Ykt6pN was similar to that of the cytoskeletal regulatory protein profilin (*16*) and is entirely different from the NH_2-terminal domain of the syntaxins [the Habc domain, which forms a three α-helical bundle (*4*–*11*)]. Although the structure of full-length Ykt6p could not be determined, elucidation of the relationship between the NH_2- and COOH-domains is essential in order to understand the function of the protein. Using a number of experimental approaches, we directly addressed this relationship.

Inspection of the molecular surface of Ykt6pN revealed a prominent hydrophobic surface on one side of the molecule comprised of several evolutionarily conserved amino acids (Phe31, Phe39, Phe42, and Phe43, see Fig. 1C and Fig. 2, A and D). This hydrophobic "patch" might represent a protein-binding surface for Ykt6pN, and despite the structural dissimilarities between Ykt6pN and syntaxin Habc, the hydrophobic surface of the core domain of Ykt6p might be a potential binding partner for Ykt6pN. Thus, we compared the $^1H,^{15}N$-HSQC (heteronuclear single-quantum coherence) spectra of Ykt6pN with those of Ykt6pNC (Ykt6pN plus the NH_2-terminal two heptad-repeats of the core domain, residues 1 to 151), and full-length Ykt6p (Fig. 2C). Consistent with a direct interaction between the core domain of Ykt6p and the NH_2-terminal domain, inclusion of the entire core domain resulted in chemical shift changes for a number of amino acid residues in the NH_2-terminal domain of the protein (Fig. 2, B and C). By using a minimal chemical shift perturbation approach (*17*), the chemical shift changes in the NH_2-domain of Ykt6p that result from interaction with its core domain were summarized (Fig. 2B). Amino acid residues from βIII and αA were involved in binding to the core domain of the protein. In contrast, no significant chemical shift changes were observed for residues in βIII and αA when Ykt6pN was extended by only two heptad-repeats into the core domain (Ykt6pNC, see Fig. 2C). Thus, the COOH-terminal part of the core domain was in direct contact with βIII and αA.

To distinguish between an inter- and an intramolecular basis for the observed interactions between the NH_2- and COOH-terminal domains of Ykt6p, we analyzed the molecular masses of Ykt6p and Ykt6pN using gel-filtration chromatography. Both Ykt6pN and Ykt6p eluted at molecular masses indicative of their being monomers, consistent with an intramolecular interaction between the core domain and the NH_2-terminal domain (Fig. 3A). In addition, gel-filtration chromatography studies revealed that the core domain of Ykt6p (residues 136 to 200) forms a high-molecular-mass aggregate (*18*). Apparently the core domain in full-length Ykt6p was sequestered, via interaction with its NH_2-domain, thereby preventing it from forming aggregates.

If the hydrophobic surface of Ykt6p (Fig. 2A) were involved in binding to the core domain of the protein, amino acid substitutions at conserved residues in this region would be expected to impair the interaction between the NH_2- and COOH-domains of Ykt6p. Indeed, substitution (*19*) of a polar

[1]Department of Biochemistry and [2]Department of Biology, The Hong Kong University of Science and Technology, Clear Water Bay, Kowloon, Hong Kong, People's Republic of China.

*These authors contributed equally to this work.
†To whom correspondence should be addressed. E-mail: bodkb@ust.hk, mzhang@ust.hk

(Gln) or charged (Glu) amino acid for Phe at Phe^{42}, or of Glu at positions Phe^{31} and Phe^{39}, resulted in loss of function of Ykt6p (Fig. 3B). Mutation of Glu for Phe at residue 42 did not alter the overall conformation of Ykt6pN, as only a few amino acid residues in the immediate vicinity of residue 42 experienced mutation-induced chemical shift changes. In contrast, a number of sharp resonances, corresponding to the amino acids in the core domain, were observed in the $^{1}H,^{15}N$-HSQC spectrum of full-length Phe42Glu-Ykt6p, suggesting that the core domain of the mutant was less structured than the wild-type protein (*18*). However, we observed significant chemical shift changes in the NH_2-terminal domain of Phe42Glu-Ykt6p (Fig. 2B) when compared with Ykt6pN, suggesting that the core and NH_2-terminal domains of the mutant protein could still interact with one another (perhaps indicative of a "semi-open" conformation). In agreement with these findings, Phe42Glu-Ykt6p had a somewhat smaller elution volume than the wild-type protein (Fig 3A).

To determine whether the altered gel-filtration profile for Phe42Glu-Ykt6p was a direct result of disruption of the intramolecular interaction between the NH_2- and COOH-termini of the protein, we used a yeast two-hybrid assay. Consistent with our prediction, the NH_2-domain of Ykt6p (residues 1 to 134) interacted with the core domain of Ykt6p (residues 136 to 200). However, the mutant NH_2-domain (Phe42Glu, residues 1 to 134) did not interact with the core domain (Fig. 3C), which is likely to be a result of disruption of the hydrophobic surface of the mutant protein. In contrast, neither the NH_2-domain nor the core domain interacted with full-length Ykt6p, presumably because of stronger intramolecular interactions between the core and the NH_2-domain in the intact protein. In agreement with this view, the NH_2-domain interacted with Phe42Glu-Ykt6p, as this amino acid substitution would alter the intramolecular association of the NH_2-domain with the core domain of Ykt6p. Thus, the nature of the interaction between the NH_2- and COOH-domains of Ykt6p was intramolecular, and alteration of this association dramatically changed the functional properties of the protein (Fig. 3). In this regard, the NH_2-domain of Ykt6p [and Habc domain of the yeast syntaxin Sso1p, (*5*)] may serve as an intramolecular chaperone for the unassembled COOH-terminal SNARE-binding core domain of the protein, as the semi-open conformational mutant, Phe42Glu-Ykt6p, is unstable in vivo (*18*). Substitution of Ala for Phe at position 42 did not result in loss-of-function or protein instability (Fig. 3F); however, Phe42Ala-ykt6 cells were cold-sensitive and exhibited defects in protein trafficking (*20*), which revealed a critical biological role for the NH_2-domain of Ykt6p (Fig. 3E).

As has been demonstrated for the yeast syntaxin Sso1p (*5*), we sought to correlate changes in the relative rates of complex assembly with mutations predicted to disrupt the closed conformation of Ykt6p. In vitro mixing experiments (*21*) revealed that relative to the wild-type protein, Phe42Glu-Ykt6p accelerated the formation of one SNARE complex about threefold (*22*) consistent with a semi-open "partially activated" conformation of the mutant protein (Fig. 3D). Although the effect of Phe42Glu-Ykt6p on SNARE complex formation was comparatively modest (*5*), the folded-back conformation of Ykt6p may play a more substantial role in the kinetics of complex formation in vivo, particularly for complexes in which the syntaxin family member does not adopt a closed conformation (*11*). Additional in vitro mixing studies revealed that Phe42Glu-Yktp6 displayed altered SNARE-pairing specificity (*20*), which suggested that contact-induced conformational changes in Ykt6p that occur upon activation of the protein may influence the specificity of SNARE-pairing (*24*, *25*) in vivo.

We have shown that the NH_2-terminal domain of the nonsyntaxin SNARE Ykt6p adopts a profilin-like fold in solution and that this domain plays a critical biological role in the function of this protein. In vitro studies revealed that alterations to the folded-back "closed" conformation of Ykt6p affected the specificity of SNARE pairing and influenced the kinetics of SNARE complex formation. Thus, Ykt6p is like some syntaxins, in that it adopts a folded-back "autoinhibited" conformation, although the NH_2-terminal domains of the two classes of SNARE proteins do not

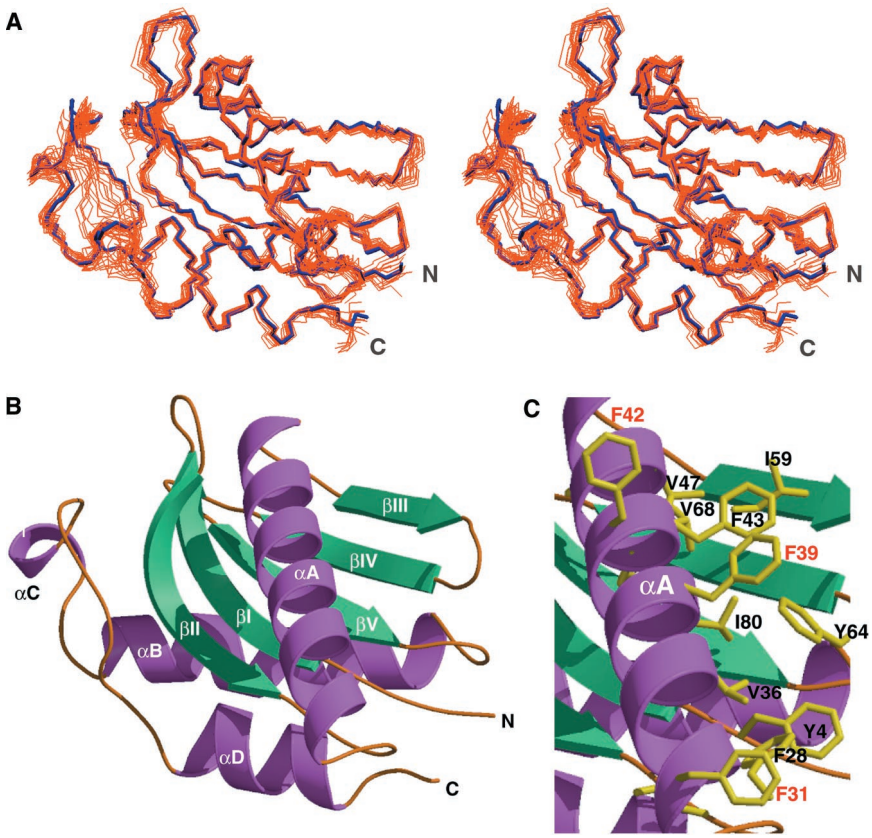

Fig. 1. Structure of the NH_2-terminal domain of Ykt6p. (**A**) Stereo view of 20 superimposed NMR-derived structures of Ykt6pN (showing the residues 1 to 133). The averaged, energy-minimized structure is represented by the thick blue lines. The root mean square deviation of the mean coordinate positions is 0.56 Å for backbones (N, C_{α}, C′) of 3 to 133 and 0.42 Å for the secondary structured regions. No distance restraints are violated by more than 0.4 Å in any of the structures, and no torsional restraints are violated by more than 5°. The Lennard-Jones potential energy for the NMR structures is -292 ± 27 kcal mol^{-1}. Procheck (*34*) analysis indicated that 97.2% of the residues are in allowed regions of the Ramachandran plot. (**B**) Ribbon representation of the averaged, minimized NMR structure of Ykt6pN. (**C**) Close-up view of the hydrophobic surface of Ykt6pN containing the conserved amino acid residues involved in binding to the core domain. Mutations in this region that lead to the loss-of-function of Ykt6p are labeled in red. Substitution of Glu for Phe30 or Ile59 results in a somewhat slower growth rate compared with the corresponding wild-type strain (see Fig. 3B). The figures were generated by using MOLMOL (*35*), MOLSCRIPT (*36*), Raster3D (*37*), and GRASP (*38*).

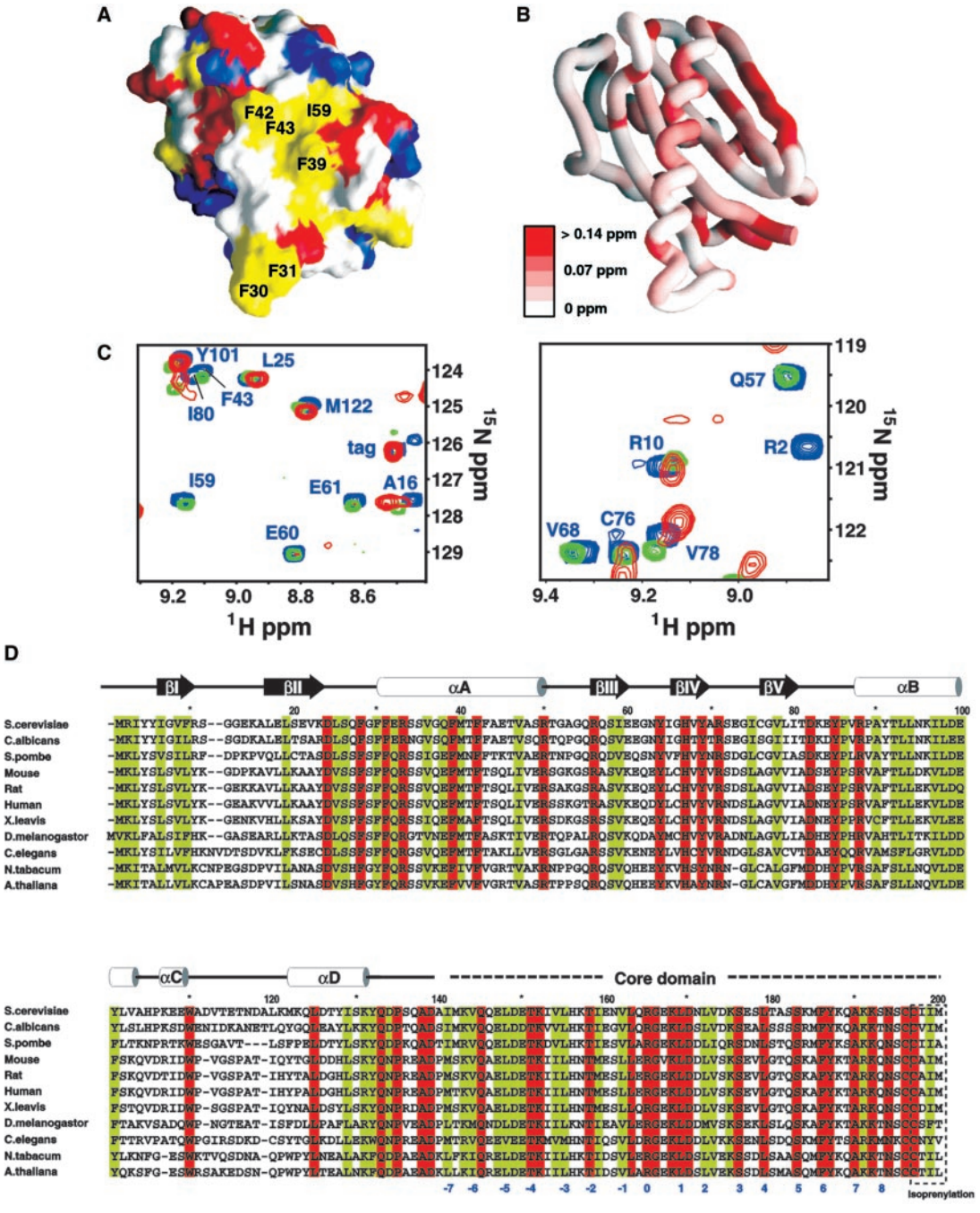

Fig. 2. Interaction of the core with the NH_2-terminal domain of Ykt6p. (**A**) The surface exposed hydrophobic surface of Ykt6pN. Lys and Arg are in blue; Asp and Glu are in red; Phe, Val, Leu, Ile, Tyr, Ala, and Trp are in yellow; all other amino acids are shown in white. The conserved hydrophobic amino acid residues are labeled. The orientation of the molecule is as shown in (B). (**B**) Summary of ^{1}H and ^{15}N combined chemical shift changes in the NH_2-domain of Ykt6p induced by the core domain. Because of the poor spectral quality of full-length Ykt6p, the shift perturbation was extracted from the ^{1}H,^{15}N-HSQC spectra of Phe42Glu-Ykt6pN and full-length, Phe42Glu-Ykt6p. (**C**) Representative regions of ^{1}H,^{15}N-HSQC spectra of Ykt6pN (blue), Ykt6pNC (green), and the full-length Ykt6p (red), showing the core domain binding-induced chemical shift changes in Ykt6pN. Inclusion of the intact core domain leads to the disappearance of a number of resonances for amino acids in βIII. In each case the concentration of the proteins used for NMR was <0.3 mM. The NMR spectra of Ykt6pN did not vary at a concentration range of 0.1 to 1.0 mM indicating that the protein chemical shift changes observed were not likely to be a result of nonspecific aggregation. (**D**) Amino acid sequence alignments of Ykt6p and its homologues. Completely conserved amino acid residues are highlighted in red, and highly conserved residues in green. The secondary structure of Ykt6pN is shown above the alignment. The heptad repeats region of the core domain is labeled as in (*39*). The isoprenylation motif of the protein is indicated by a dashed open box. The NCBI accession numbers of the proteins are *Saccharomyces cerevisiae* (NP012725), *Candida albicans* (CAA21982), *Schizosaccharomyces pombe* (CAA18664), mouse (NP062635), rat (AAD09152), human (NP006546), *Xenopus leavis* (AAC32182), *Drosophila melanogastor* (AAF46294), *Caenorhabditis elegans* (AAD31930), *Nicotiana tabacum* (AAD00116), and *Arabidopsis thaliana* (AAD00112).

share any structural similarity. Autoinhibitory regulation may therefore be a universal feature of SNARE-SNARE interactions. Indeed, for SNAREs, which have domains in addition to the SNARE-binding core and which function in multiple transport steps, an autoinhibitory mechanism that permits temporal and spatial kinetic control of cognate SNARE complex assembly seems likely. Amino acid sequence analysis and structure prediction of another nonsyntaxin SNARE, Sec22p (*3*), indicated that its NH_2-terminal domain is likely to adopt a fold similar to that of Ykt6pN. While this manuscript was under review, the crystal structure of the NH_2-domain of mouse Sec22b was published, supporting our prediction (*26*).

References and Notes

1. J. E. Rothman, *Nature* **372**, 55 (1994).
2. R. Jahn, T. C. Südhof, *Annu. Rev. Biochem.* **68**, 863 (1999).
3. H. R. Pelham, *Exp. Cell Res.* **247**, 1 (1999).
4. I. Fernandez *et al.*, *Cell* **94**, 841 (1998).
5. M. Munson, X. Chen, A. E. Cocina, S. M. Schultz, F. M. Hughson, *Nature Struct. Biol.* **7**, 894 (2000).
6. K. L. Nicholson *et al.*, *Nature Struct. Biol.* **5**, 793 (1998).
7. K. M. Fiebig, L. M. Rice, E. Pollock, A. T. Brunger, *Nature Struct. Biol.* **6**, 117 (1999).
8. J. C. Lerman, J. Robblee, R. Fairman, F. M. Hughson, *Biochemistry* **39**, 8470 (2000).
9. K. M. Misura, R. H. Scheller, W. I. Weis, *Nature* **404**, 355 (2000).
10. I. Dulubova *et al.*, *EMBO J.* **18**, 4372 (1999).
11. I. Dulubova, T. Yamaguchi, Y. Wang, T. C. Südhof, J. Rizo, *Nature Struct. Biol.* **8**, 258 (2001).

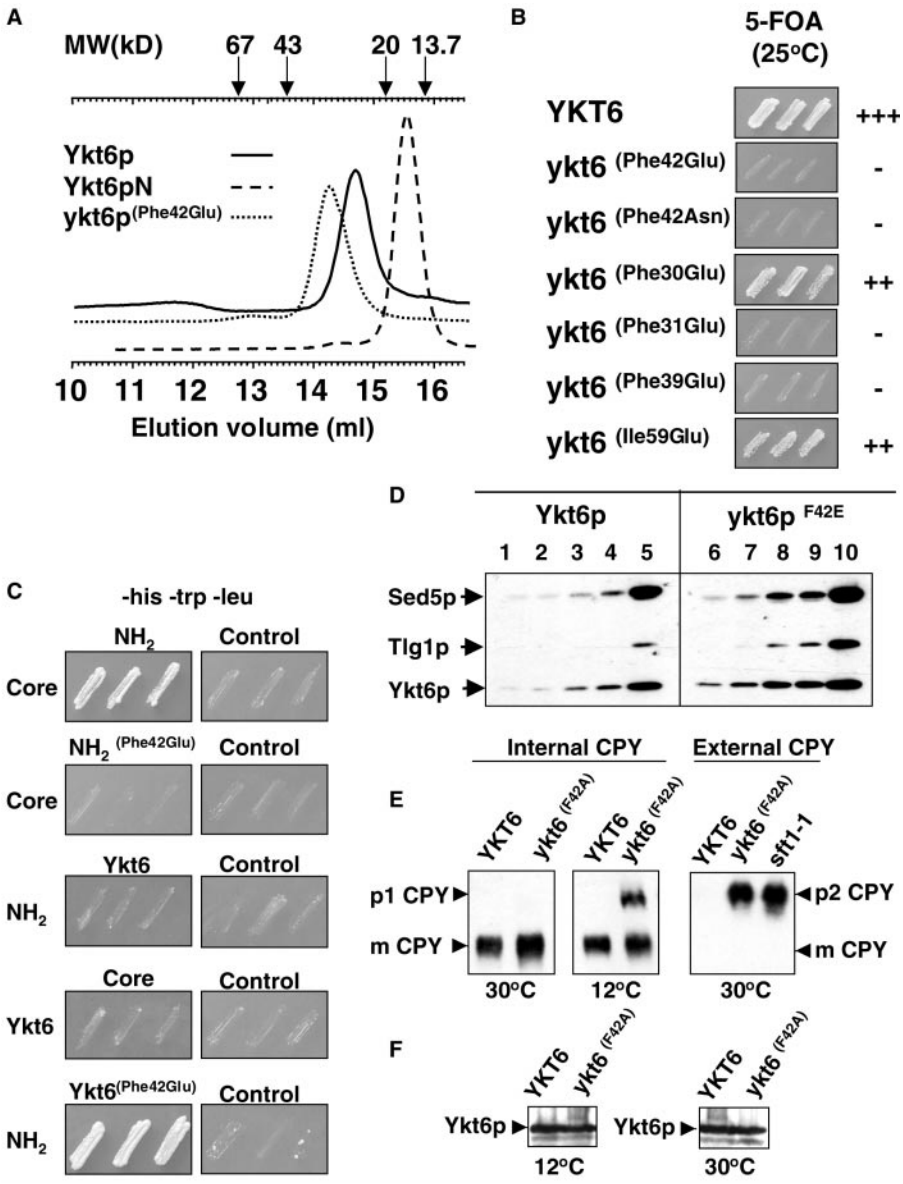

Fig. 3. The NH_2-terminal domain of Ykt6p sequesters its core domain and is important for function. (**A**) Gel-filtration analysis showing that both Ykt6pN and Ykt6p exist as monomers in solution. The elution volumes of molecular mass standards are indicated on the top of the panel. The column buffer was identical to that used in NMR experiments and the concentration of the proteins was in the range of 0.02 to 0.15 mM. (**B**) Viability of yeast strains expressing mutant forms of Ykt6p. SARY158 cells [*ykt6*Δ pYKT6, see (*14*)] containing various ykt6 mutants were patched onto media containing 5-FOA. Lack of growth on 5-FOA indicates that the particular mutant cannot suffice as the sole source of Ykt6p. The plus symbols (+) indicate the relative growth rates of SARY158 cells expressing ykt6 mutant proteins as their sole source of Ykt6 protein where +++ is wild type, and – is no growth. (**C**) The NH_2-domain of Ykt6p interacts with its core domain in the two-hybrid system. Core domain, NH_2-domain, and full-length Ykt6p in bait vector were tested against wild-type NH_2-domain, mutant (Phe42Glu) NH_2-domain, and full-length wild-type Ykt6p or Phe42Glu-Ykt6p in prey vector. Empty prey vector was used as a control. (**D**) Phe42Glu-Ykt6p accelerates SNARE-complex formation in vitro. GST-Vti1p was incubated with $(His)_6$-Sed5p (25 μg) and $(His)_6$-Tlg1p (8 μg) together with either Ykt6p or Phe42Glu-Ykt6p (25 μg) at 4°C for 15 min, 30 min, 60 min, 120 min, or 22 hours (lanes 1 to 5 and 6 to 10, respectively). (**E**) Substitution of Ala for Phe at position 42 in the N-domain of Ykt6p results in defects in protein trafficking (*20*). $ykt6^{Phe42Ala}$ cells accumulate p1 carboxypeptidase Y (CPY) at 12°C and miss-sort p2 CPY at 30°C. mCPY (mature form), p1 CPY (endoplasmic reticulum–modified form), p2 CPY (Golgi-modified form). (**F**) Phe42Ala-ykt6p is stable. Phe42Ala-ykt6 and wild-type (YKT6) yeast strains were grown at 12°C or 30°C to an optical density OD_{660} of 0.6 and 1.5 OD_{660} equivalents of total yeast protein were assayed by immunodetection with antibodies against Ykt6p.

12. J. A. McNew *et al.*, *J. Biol. Chem.* **272**, 17776 (1997).
13. C. Ungermann *et al.*, *J. Cell Biol.* **145**, 1435 (1999).
14. M. M. Tsui, D. K. Banfield, *J. Cell Sci.* **113**, 145 (2000).

15. The polymerase chain reaction (PCR)–amplified NH_2-terminal domain (residues 1 to 140, Ykt6pN), full-length Ykt6p (residues 1 to 200), and various mutants of the protein were subcloned into a modified version of pET32 vector (Novagen) termed pET32H (in which the S-tag and enterokinase cleavage encoding DNA sequences were removed). Amino acid substitutions in Ykt6p were generated by site-directed mutagenesis (*27*). Thioredoxin-fused, His-tagged Ykt6pN was expressed in *Escherichia coli* BL21(DE3) cells, and the fusion protein was purified by using a Ni^{2+}-nitrilotriacetic acid (NTA) affinity column. The NH_2-terminal thioredoxin His-tagged peptide fragment was cleaved by digesting the fusion protein with thrombin, and Ykt6pN was purified by gel filtration. Uniformly ^{15}N- and $^{15}N/^{13}C$-labeled Ykt6p proteins were prepared by growing the bacteria in M9 minimal medium containing $^{15}NH_4Cl$ with or without $^{13}C_6$-glucose. NMR samples contained ~1.0 mM of Ykt6pN in 100 mM potassium phosphate, pH 6.0, 5 mM d_{10}-DTT (dithiothrietol) in 90% H_2O and 10% D_2O or 99.9% D_2O. NMR spectra were acquired at 30°C on a Varian Inova 750-MHz spectrometer. Sequential backbone and nonaromatic, nonexchangeable side-chain resonance assignments of the protein were obtained by standard heteronuclear correlation experiments (*28*, *29*). The side chains of aromatics were assigned by ^1H two-dimensional (2D) total correlation spectroscopy with nuclear Overhauser effect spectroscopy (TOCSY/NOESY) experiments of an unlabeled protein sample in D_2O. The stereospecific assignment of the Val and Ile methyl groups was obtained by using a 10% ^{13}C-labeled sample (*30*). Approximate interproton distance restraints were derived from NOESY spectra (a ^1H 2D homonuclear NOESY, a ^{15}N-separated-NOESY and a ^{13}C-separated NOESY). NOEs were grouped into three distance ranges 1.8 to 2.7 Å (1.8 to 2.9 Å for NOEs involving NH protons), 1.8 to 3.3 Å (1.8 to 3.5 Å for NOEs involving NH protons), and 1.8 to 5.0 Å, corresponding to strong, medium, and weak NOEs. Hydrogen bonding restraints (two per hydrogen bond where $r_{NH\text{-}O} = 1.8$ to 2.2 Å and $r_{N\text{-}O} = 2.2$ to 3.3 Å) were generated from the standard secondary structure of the protein on the basis of the NOE patterns and the backbone secondary chemical shifts. Backbone dihedral angle restraints (ϕ and ψ angles) were derived from $^3J_{HN\alpha}$ coupling constants measured by using an HNHA experiment and backbone chemical shift analysis program TALOS (*31*). Structures were calculated by using the program CNS (*32*).

16. N. M. Mahoney, P. A. Janmey, S. C. Almo, *Nature Struct. Biol.* **4**, 953 (1997).
17. B. T. Farmer *et al.*, *Nature Struct. Biol.* **3**, 995 (1996).
18. H. Tochio, M. M. K. Tsui, D. K. Banfield, M. Zhang, unpublished data.

19. All yeast strains were grown at 25°C or 30°C in yeast extract–peptone–dextrose (YEPD) medium, or in synthetic dextrose medium lacking the appropriate amino acids, or on plates containing 5-fluoro-orotic acid (5-FOA, 100 μg/ml) as appropriate. Standard yeast molecular genetic techniques were carried out as described previously (*14*, *24*). The LexA two-hybrid system was used together with the yeast reporter strain EGY48 (*MAT*α his3 trp1 leu2::pLEU2-LEXAop3) and the bait (pEG202) and prey plasmids (pJG4-5) (*33*). The full-length fusions of Ykt6p and Phe42Glu-Ykt6p comprised residues 1 to 200, the NH_2-domain fusion comprised residues 1 to 134 of Ykt6p, and the core fusion comprised residues 136 to 200. To access the two-hybrid interaction, each experiment was repeated at least three times.
20. Yeast strains (*24*) were grown in YEPD for 4 hours at 30°C or for 20 hours at 12°C. Internal and secreted (external) protein samples were prepared and processed as described in (*14*). Equivalent amounts of internal and secreted proteins were analyzed from the wild-type and mutant strains.

21. The $(His)_6$-ykt6$^{(Phe42Glu)}$p expression construct was generated by replacing the wild-type *YKT6* fragment from $(His)_6$-Ykt6p with the corresponding fragment of *ykt6* (encoding ykt6$^{(Phe42Glu)}$p). SNARE binding assays were performed essentially as described previously (*14*, *24*). Purified recombinant SNARE proteins were added to the washed GST-Vti1p bead slurry in a final volume of 750 μl. $(His)_6$-Sed5p and $(His)_6$-Tlg1p were detected by immunostaining with an antibody against His_6 (*14*, *24*) and Phe42Glu-Ykt6p was detected by immunostaining with affinity-purified Ykt6p antiserum.
22. Band intensity was converted to arbitrary units by densitometry. The initial relative velocities at which Sed5p and Ykt6p were incorporated into the SNARE complex were determined from the slopes obtained by plotting arbitrary units against time. This was done for the data points up to and including 60 min (for Phe42Glu-Ykt6p) and 120 min (for Ykt6p), during which time the velocity was found to be constant. The relative differences in the observed velocities were expressed as a ratio of the Phe42Glu/Wild-type slopes.
23. Supplementary material is available on *Science* Online at www.sciencemag.org/cgi/content/full/293/5530/698/DC1.
24. M. M. Tsui, W. C. S. Tai, D. K. Banfield, *Mol. Biol. Cell* **12**, 521 (2001).
25. J. A. McNew *et al.*, *Nature* **407**, 153 (2000).
26. L. C. Gonzalez Jr., W. I. Weis, R. H. Scheller, *J. Biol. Chem.* **276**, 24203 (2001).
27. T. A. Kunkel, *Proc. Natl. Acad. Sci. U.S.A.* **82**, 488 (1985).
28. A. Bax, S. Grzesiek, *Acc. Chem. Res.* **26**, 131 (1993).
29. G. M. Clore, A. M. Gronenborn, *Trends Biotechnol.* **16**, 22 (1998).
30. D. Neri, T. Szyperski, G. Otting, H. Senn, K. Wuthrich, *Biochemistry* **28**, 7510 (1989).
31. G. Cornilescu, F. Delaglio, A. Bax, *J. Biomol. NMR* **13**, 289 (1999).
32. A. T. Brunger *et al.*, *Acta Crystallogr. D Biol. Crystallogr.* **54**, 905 (1998).
33. E. A. Golemis, J. Gyuris, R. Brent, *Interaction Trap/Two Hybrid System to Identify Interacting Proteins* (Wiley, New York, 1996), pp. 20.1.1–20.1.28.
34. R. A. Laskowski, J. A. Rullmannn, M. W. MacArthur, R. Kaptein, J. M. Thornton, *J. Biomol. NMR* **8**, 477 (1996).
35. R. Koradi, M. Billeter, K. Wuthrich, *J. Mol. Graph.* **14**, 51 (1996).
36. P. J. Kraulis, *J. Appl. Crystallogr.* **24**, 946 (1991).
37. E. Merritt, M. Murphy, *Acta Crystallogr.* **D50**, 869 (1994).
38. A. Nicholls, *GRASP: Graphical Representation and Analysis of Surface Properties* (Columbia Univ. Press, New York, 1992).
39. R. B. Sutton, D. Fasshauer, R. Jahn, A. T. Brunger, *Nature* **395**, 347 (1998).
40. We thank F. Hung and Q. Zhang for assistance in protein purification and gel-filtration experiments, respectively, and C. Rock for comments on the manuscript. This work was supported by grants from the Research Grant Council of Hong Kong to D.K.B and M.Z. and by a grant from the Human Frontiers Science Program Organization to M.Z. The NMR spectrometer used in this work was purchased with funds donated to the Biotechnology Research Institute by the Hong Kong Jockey Club. The coordinates of the structure of Ykt6pN have been deposited in the Protein Data Bank (accession code 1h8m).

30 May 2001; accepted 5 June 2001

Lysophosphatidylcholine as a Ligand for the Immunoregulatory Receptor G2A

Janusz H. S. Kabarowski,[1]* Kui Zhu,[2]* Lu Q. Le,[1] Owen N. Witte,[1,3]† Yan Xu[2,4]†

Although the biological actions of the cell membrane and serum lipid lysophosphatidylcholine (LPC) in atherosclerosis and systemic autoimmune disease are well recognized, LPC has not been linked to a specific cell-surface receptor. We show that LPC is a high-affinity ligand for G2A, a lymphocyte-expressed G protein–coupled receptor whose genetic ablation results in the development of autoimmunity. Activation of G2A by LPC increased intracellular calcium concentration, induced receptor internalization, activated ERK mitogen-activated protein kinase, and modified migratory responses of Jurkat T lymphocytes. This finding implicates a role for LPC-G2A interaction in the etiology of inflammatory autoimmune disease and atherosclerosis.

Lysophospholipids regulate a variety of biological processes including cell proliferation, tumor cell invasiveness, and inflammation (*1*, *2*). LPC, produced by the action of Phospholipase A_2 (PLA_2) on phosphatidylcholine, promotes inflammatory effects, including increased expression of endothelial cell adhesion molecules and growth factors (*3*, *4*), monocyte chemotaxis (*5*), and macrophage activation (*6*). As a component of oxidized low density lipoprotein (oxLDL), LPC plays an etiological role in atherosclerosis (*7*) and is implicated in the pathogenesis of the autoimmune disease systemic lupus erythematosus (SLE) (*8*). Despite physiologically high concentrations in body fluids (up to 100 μM) (*9*), extracellular actions of LPC through G protein–coupled receptors (GPCRs) are indicated (*10*, *11*). Although LPC action through a platelet activating factor (PAF) receptor(s) has been suggested (*10*, *11*), a specific LPC receptor has yet to be identified. OGR1 is a high-affinity receptor for sphingosylphosphorylcholine (SPC), a lysophospholipid structurally similar to LPC (*12*). OGR1 is closely related to G2A (*13*), TDAG8 (*14*), and GPR4 (*15*). G2A is a transcriptionally regulated GPCR expressed predominantly in lymphocytes, and its expression in response to stress stimuli and prolonged mitogenic signals suggests that it may negatively regulate lymphocyte growth (*13*). Genetic ablation of G2A function in mice further indicates a role for G2A in the homeostatic regulation of lymphocyte pools and autoimmunity (*16*).

To determine if G2A is a lysophospholipid receptor, we assessed signaling responses in cells ectopically expressing G2A (*17*). Human breast epithelial MCF10A cells were used because they do not express G2A or OGR1, and do not respond to SPC (*12*). Intracellular calcium concentration ($[Ca^{2+}]_i$) was determined in MCF10A cells that were transfected with plasmids encoding green fluorescent protein–tagged G2A (G2A.GFP) (*18*) or GFP (*19*). LPC and SPC (0.1 μM) treatment induced transient $[Ca^{2+}]_i$ increases in G2A.GFP expressing cells only. Responses to lysophosphatidic acid (LPA) (1 μM), PAF (0.1 μM), and adenosine triphosphate (ATP) (20 μM) were not affected by G2A expression (Fig. 1A). Dose-dependent increases in $[Ca^{2+}]_i$ were observed in G2A.GFP-expressing cells [LPC, median effective concentration (EC_{50}) ~0.1 μM; SPC, EC_{50} ~0.4 μM] (Fig. 1B). Pretreatment of G2A.GFP-expressing cells with the PAF receptor antagonist BN 52021 (200 μM) blocked $[Ca^{2+}]_i$ elevation induced by PAF, but not that induced by LPC (1 μM), SPC (1 μM), LPA (1 μM), or ATP (20 μM) (Fig. 1C), indicating that LPC and SPC did not act through a PAF receptor. The pretreatment of G2A.GFP-expressing cells with LPC (1 μM) or SPC (10 μM) induced desensitization to subsequent stimulation with either agonist (1 μM) (Fig. 1D).

When G2A.GFP-expressing cells were pretreated with pertussis toxin (PTX, 100 ng/ml), an inhibitor of $G\alpha_i$, transient $[Ca^{2+}]_i$ increases induced by LPA (1 μM), LPC (0.1 to 5 μM), and SPC (1 to 5 μM) were inhibited (Fig. 1E). Calcium transients elicited by PAF (0.1 μM) or ATP (20 μM) were not affected. Pretreatment of

[1]Department of Microbiology, Immunology, and Molecular Genetics; [2]Department of Cancer Biology, Lerner Research Institute, 9500 Euclid Avenue, Cleveland, OH 44195, USA. [3]Howard Hughes Medical Institute, University of California Los Angeles, Los Angeles, CA 90095–1662, USA. [4]Department of Gynecology and Obstetrics, Cleveland Clinic Foundation, 9500 Euclid Avenue, Cleveland, OH 44195, USA.

*These authors contributed equally to this work.
†To whom correspondence should be addressed. E-mail: owenw@microbio.ucla.edu (O.N.W.); xuy@ccf.org (Y.X.)